Influence of shear and compressive stress regimes on efficient $NaBH_4$ mechanochemical regeneration

Garrido Nuñez, Santiago; Schott, Dingena L.; Padding, Johan T.

DOI
10.1016/j.cej.2025.170168

Publication date
2025

Document Version
Final published version

Published in
Chemical Engineering Journal

Citation (APA)
Garrido Nuñez, S., Schott, D. L., & Padding, J. T. (2025). Influence of shear and compressive stress regimes on efficient $NaBH_4$ mechanochemical regeneration. *Chemical Engineering Journal*, *525*, Article 170168. https://doi.org/10.1016/j.cej.2025.170168

Chemical Engineering Journal 525 (2025) 170168

Contents lists available at ScienceDirect

Chemical Engineering Journal

journal homepage: www.elsevier.com/locate/cej

Influence of shear and compressive stress regimes on efficient $NaBH_4$ mechanochemical regeneration

Santiago Garrido Nuñez [a,*], Dingena L. Schott [b], Johan T. Padding [a]

[a] Department of Process and Energy, Delft University of Technology, Leeghwaterstraat 39, Delft, 2628 CB, The Netherlands
[b] Department of Maritime and Transport Technology, Delft University of Technology, Mekelweg 2, Delft, 2628 CD, The Netherlands

ARTICLE INFO

Keywords:
Ball milling
Discrete element method
Mechanochemistry
Sodium borohydride
Hydrogen

ABSTRACT

We compare the influence of tangential (shear) and normal (compressive) stress events on the mechanochemical regeneration of sodium borohydride $NaBH_4$ from hydrated sodium metaborate $NaBO_2 \cdot 4\,H_2O$ and magnesium hydride MgH_2. Discrete element method (DEM) mechanical descriptors are used to design experiments that either maintain the mill at a constant rotational speed or maintain a constant total dissipation power, thereby separating stress distribution from net power input. Under constant power operation, a tangential rich regime achieves a record 94% conversion yield with 37.5% shorter milling time, 40% lower ball-to-powder ratio, and 34% reduced speed. However, this high yield requires such a substantial power consumption that the converted mass per Watt drops to only 0.090 g W^{-1}, below both balanced (0.113 g W^{-1}) and normal-bias (0.108 g W^{-1}) cases. By contrast, a tangential bias at half the power (3 W) still delivers 84% yield and peaks at 0.185 g W^{-1}, illustrating the often disregarded trade-off between absolute conversion and energetic productivity in mechanochemistry. Specific yield (conversion per Watt) likewise peaks at 0.28 W^{-1} and declines linearly with fill ratio ($R^2 > 0.99$). Mechanochemical energy leverage analysis reveals that, at most, 1.7–3.7% of input mechanical work is theoretically recoverable on an enthalpy basis, 2.1–4.4% on a Gibbs free energy basis, and 4–8.7% when considering the fuel value of all available hydrogen. Our mill-agnostic framework provides a transferable blueprint for cross-platform optimization of mechanochemical processes.

1. Introduction

Sodium borohydride ($NaBH_4$) is an attractive solid hydrogen carrier given its high theoretical energy density and gravimetric hydrogen storage [1,2]. The hydrolysis of $NaBH_4$ releases hydrogen and produces sodium metaborate ($NaBO_2 \cdot xH_2O$) as a byproduct:

$$NaBH_4 + (2 + x)H_2O \rightarrow NaBO_2 \cdot xH_2O + {}_4H_2 \quad (1)$$

where x is the level of hydration.

The central barrier to the deployment of sodium borohydride at scale is not the hydrogen release, but rather its regeneration. In 2007, the U.S. Department of Energy (DOE) go/no-go reviews concluded that all assessed $NaBH_4$ pathways exceeded cost targets primarily due to high regeneration costs and sodium price sensitivity, leading to a no-go recommendation for on-board hydrolysis [3]. Since then, $NaBH_4$ mechanochemical loops have co-integrated hydrogen release and regeneration within a single, solvent-free process window by capturing the hydrolyzate as borates/carbonates and solid-state reducing it back to $NaBH_4$ under ambient milling. The approach bypasses high-pressure H_2, compression, solvent use, and dehydration, consistently achieving ~70%–80% regeneration yield [4–9]. Relevant examples in the context of this work are shown in Table 1.

Analogous one-step variants have been demonstrated for $LiBH_4$ and $Mg(BH_4)_2$, underscoring that mechanochemistry enables new opportunities for process integration and cost reduction across complex hydrides [10–13]. We also note a related mechanochemical route to $NaBH_4$ from $NaB(OH)_4$ using Mg–Al intermetallics; reported yields remain comparatively low under prolonged milling (<~43%), reflecting different interfacial chemistry than the MgH_2-driven cycles considered here [14]. In previous research, we have presented results of the mechanochemical regeneration of $NaBH_4$ from a system comprising $NaBO_2 \cdot 4\,H_2O$ and MgH_2 (Eq. (2)) with yields reaching up to 90% along with a ranking of the operational variables (rotational speed, milling time, ball-to-powder ratio and molar ratio) based on their relevance to the chemical yield, with milling time being the most significant [15].

$$NaBO_2 \cdot 4\,H_2O + {}_6MgH_2 \rightarrow NaBH_4 + {}_6MgO + {}_8H_2 \quad (2)$$

* Corresponding author.
E-mail address: s.garridonunez@tudelft.nl (S. Garrido Nuñez).

https://doi.org/10.1016/j.cej.2025.170168
Received 31 July 2025; Received in revised form 9 October 2025; Accepted 25 October 2025
Available online 30 October 2025

Table 1
Reported results of the mechanochemical regeneration of $NaBH_4$.

Metaborate	2nd reactant	Reported yield (%)	Year	Ref.
$NaBO_2$	MgH_2	76	2009	[21]
$NaBO_2$	MgH_2	71	2009	[22]
$NaBO_2$	MgH_2	74	2011	[23]
$NaBO_2$	MgH_2	89	2017	[24]
$NaBO_2 \cdot 2H_2O$	Mg	68	2017	[25]
$NaBO_2 \cdot 2H_2O$	MgH_2	90	2017	[26]
$NaBO_2 \cdot 4H_2O$	MgH_2	88	2017	[26]
$NaBO_2 \cdot 2H_2O$	Mg_2Si	78	2017	[5]

More generally, mechanochemistry harnesses mechanical energy to drive chemical transformations, but its practice often treats the applied stresses simplistically (e.g., as a pressure or scalar force) rather than as a full stress tensor [16,17]. In reality, mechanical loading in ball milling involves both normal (compressive) and tangential (shear) stress components. The distinct roles of these stress modes, however, have rarely been explored in mechanochemical studies. Apart from a few targeted studies, most notably Kobayashi et al. [18] who mapped the spatial distribution of normal and tangential stresses for a single ball in a planetary ball mill, most reports and mechanistic studies treat mechanical loading as a single pressure or force magnitude, overlooking the fact that shear and compression can influence reaction pathways differently [16,19]. For example, the Bell model expresses the rate enhancement via a term $\exp\left(-\frac{P\Delta V}{RT}\right)$ involving an isotropic pressure P, but effectively ignores any anisotropy [19]. This simplification means that chemically important distinctions, for example, that tensile stress tends to break bonds, while normal stress often drives bond formation, can be overlooked [20].

Indeed, several authors point out that common methodologies lack independent control of stress modes. For example, studies of boundary lubrication films (ZDDP tribofilm growth) show that prior experiments based on tribometers could not independently control the normal and tangential stress [27]. Quantitative comparisons further underscore the oversight: for ZDDP tribofilm formation, the measured activation volume under shear loading (~0.18 nm^3) is nearly twenty times larger than that under pure compression (~0.01 nm^3), confirming that tangential, not normal stress, drives the mechanochemical reaction [27].

Several factors contribute to this oversimplification. On the experimental side, it is difficult to apply or measure pure shear without collateral normal forces. Most common mechanochemical reactors (ball mills, twin-screw extruders) impose mixed stress states. For instance, planetary and high-energy ball mills induce both impact, and shear forces; continuous extruders force material through narrow channels applying high tangential and normal stress simultaneously [28]. Few laboratory techniques allow independent control of shear versus compression. Traditional pressure devices (diamond-anvil cells, gas- or liquid-pressure cells, AFM tips) primarily deliver uniform normal stress, while tribometers typically combine tangential and normal loading [16]. Even with these limited experimental options, conclusions drawn under such idealized conditions remain difficult to generalize to bulk mechanochemical operations, where complex, varying stress landscapes deviate from bench-top experiments. A consequence of this is that well-defined shear loading is rarely isolated in mechanochemical experiments, so mechanisms driven by sliding or frictional forces are usually inferred indirectly [28].

In summary, both experimental practice and theoretical frameworks have treated mechanical loading as effectively scalar, bypassing the need to decouple components. These simplifications have significant implications. By ignoring stress anisotropy, predictive models may fail to capture important mechanistic pathways. For instance, Jonas et al. showed that under pure sliding (shear) conditions, there exists a finite critical stress below which no reaction occurs, contrary to the continuous behavior predicted by the scalar Bell model [19]. If one calibrates a model on compression-induced data, it may not predict shear-driven kinetics correctly. Similarly, an experimental result obtained under one loading mode (e.g., hydrostatic press) may not translate to another (e.g., milling) if the shear contribution is different, leading to a misinterpretation of which bonds are activated. Moreover, because mills can operate under different principles, there is broad variation in collision frequencies, impact energies, and shear rates, rendering comparative evaluation across milling platforms complicated [29–33]. This lack of detail can also hamper reactor design when up-scaling becomes relevant; without knowing how shear or normal forces drive a transformation, it is hard to optimize milling media, extruder screw profiles, or frictional conditions to maximize yield or selectivity. In practice this could mean, for example, that some reaction products remain inaccessible simply because the wrong stress component is being applied. Overall, neglecting shear–normal distinctions reduces the predictive power of mechanochemical models and can obscure the true mechanism of activation.

A concrete example relevant to the context of this work is the regeneration of $NaBH_4$. Research has focused on trying different reducing agents or hydration levels while attempting to maximize yield within a limited set of operational parameters (rotational speed, ball-to-powder ratio (BPR), milling time, and molar ratio) [5,21–26]. Unfortunately, this has unintentionally diverted attention from a deeper understanding of the mechanical system that defines the success of the reaction [34]. This presents several challenges: reproducibility becomes problematic unless identical equipment is used, scaling-up becomes challenging, the connection between macroscopic behavior and molecular transformations is neglected, and predictive models that allow quantitative descriptions of expected chemical conversion are scarce [35]. As reported in our previous study [15], the intended replication of identical operational parameters in a different ball mill (for example, going from a shaker ball mill to a high-energy ball mill) led to completely different results in the mechanochemical regeneration of $NaBH_4$. Thus, given the fundamental changes in design, operation, and energy input of different mills, it becomes evident that these operational parameters are not sufficient to accurately characterize a mechanochemical process if the ultimate goals are increasing efficiency, scaling-up, and ensuring reproducibility across devices. To overcome the shortcomings outlined above, namely poor interlaboratory reproducibility, the inability to decouple normal and tangential stress modes, and the resulting obstacles to reliable scale-up, we proposed and validated a methodology that characterizes mechanochemical processes by analyzing the mechanical interactions occurring inside the milling jar through Discrete Element Method (DEM) modeling [36,37]. By defining three characteristic values: the mean normal energy dissipation per collision, $\bar{E}_n$; the mean tangential energy dissipation per collision, $\bar{E}_t$; and the specific collision frequency, f_{col}/n_{ball}, we could successfully predict the chemical yield of $NaBH_4$ regeneration under previously untested operational conditions. Together, these metrics capture the distribution of energy dissipated between normal and tangential contacts, providing a practical representation for the underlying stress landscape in a bulk mechanochemical process because the energy released in each collision scales directly with the normal or tangential force components; partitioning that energy therefore mirrors how compressive and shear stresses are delivered in the jar.

Because these descriptors are derived directly from particle–particle and particle–wall interactions, they remain independent of the mill's working principle and design. Consequently, any milling device that can reproduce the triplet $\{\bar{E}_n, \bar{E}_t, f_{col}/n_{ball}\}$ should deliver the expected chemical conversion. Moreover, since the framework explicitly separates the contributions of compression (normal interactions) and shear (tangential interactions), it gives the unique opportunity to deliberately tune their balance in the system while keeping the total mechanical power dissipation constant. Since this power can be expressed as $(\bar{E}_n + \bar{E}_t)\, f_{col}$, the mechanical descriptors can be manipulated to maintain an invariant mechanical 'budget' even as the fill ratio (i.e. the volume occupied by the balls divided by the jar's total internal

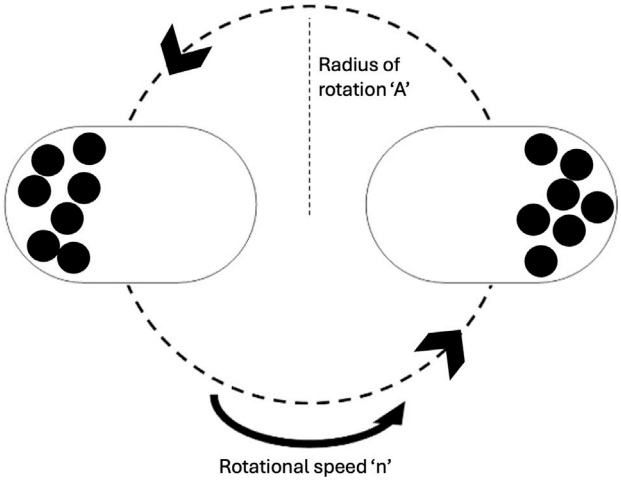

Fig. 1. Schematic of jar movement. Figure reused from Garrido et al. [15], International Journal of Hydrogen Energy, 2025. This article is licensed under a Creative Commons Attribution 4.0 International License (CC BY 4.0).

volume) changes, and hence the grinding media mass and internal dynamics. The master-curve framework provides the compensating adjustments in rotational speed or amplitude required to hold that power fixed while smoothly shifting the ratio $\bar{E}_t/\bar{E}_n$ from shear-dominated to compression-dominated regimes. This decouples the stress mode from net energy delivery, allowing mechanistic comparisons that are free from confounding effects and isolating the true influence of shear versus normal loading on reaction kinetics. Moreover, projecting any milling device onto the same $\{\bar{E}_n, \bar{E}_t, f_{\mathrm{col}}/n_{\mathrm{ball}}\}$ space yields a quantitative stress fingerprint that immediately reveals whether the mill intrinsically favors shear or compression, providing a rigorous, transferable basis for equipment benchmarking, optimization, and scale-up.

2. Model and materials

The Emax high-energy ball mill, distributed by the German company Retsch, is used for all experiments. The system was set up to allow a maximum temperature of 50 °C. The machine allocates proprietary grinding jars with 125 mL of volume that follow a circular motion with a rotational speed n up to 2000 revolutions per minute with an amplitude (radius) A of 1.7 cm, see Fig. 1.

Hydrated sodium metaborate ($NaBO_2 \cdot 4\,H_2O$) (≥99%) was purchased from Sigma-Aldrich, while magnesium hydride (MgH_2) (≥99.9%, ≤50 μm) was obtained from Nanoshel. All reactants were used without further purification. The sample preparation for ball milling was carried out in a glovebox under an argon atmosphere, with oxygen and water concentrations maintained below 0.1 ppm. For a detailed description of the quantification of chemical yield and the cleaning of the equipment to preserve similar conditions for all experimental cases, we refer to our previous work [15].

2.1. Modeling approach and case definition

The interactions between the milling jar and the grinding media were modeled and simulated using the Discrete Element Method (DEM). For this study, Altair EDEM 2021.2 was used as DEM solver, while Python 3.9.12 was used for data post-processing. EDEM implements a soft-sphere approach, calculating particle contact forces based on the Hertz–Mindlin model. We refer to our previous work [36] for a detailed description of the contact model and the equations governing the particle's motion in the DEM framework, as well as for the calibration and data post-processing carried out to produce the master curves presented in Fig. 2.

The master curves (Fig. 2(a) and (b)) represent the expected mechanical action of the high-energy ball mill in terms of mean specific power dissipation in the normal and tangential directions, respectively. Additionally, the specific collision frequency and ratio between both modes of dissipation are also presented (Fig. 2(c) and (d)). These master curves were obtained from a large number of DEM simulations, normalizing the measured dissipated energies and collisions through Eqs. (3) and (4).

$$\tilde{P}_{spec} = \frac{f_{col}\,\bar{E}_{n,t}}{\rho\omega^3 A^2 d_p^3 n_{ball}} \tag{3}$$

$$\tilde{f}_{col} = \frac{f_{col}}{\omega n_{ball}} \tag{4}$$

where ρ is the milling ball density, ω is the rotational speed of the mill, A is the amplitude of oscillation, d_p is the diameter of the milling balls, and n_{ball} is the number of milling balls in the system.

The combination of the master curves along with Eqs. (3) and (4) enables the estimation of the triplet of characteristic values ($\bar{E}_n$, $\bar{E}_t$ and f_{col}/n_{ball}) for this mechanochemical process without the need for any simulations. Then, it is possible to calculate the total power following Eq. (5).

$$P_{tot} = f_{\mathrm{col}}\left(\bar{E}_n + \bar{E}_t\right) \tag{5}$$

Looking at the ratio between tangential and normal dissipation (Fig. 2(d)), it becomes possible to define three distinct operational regimes that strictly depend on the fill ratio. The first goes from 4% to 9% fill ratio and favors tangential dissipation. At 10%, an elbow can be identified in the curve, meaning that this fill ratio provides the best balance between normal and tangential dissipation in this mill. Then, the second zone, which extends up to 20%, increases the relevance of normal dissipation. Lastly, the third zone, extending beyond 20%, provides no benefit as the ratio can no longer achieve values beyond those achievable at lower fill ratios. Thus, to test the effect of each mode of dissipation on the mechanochemical yield, the cases presented in Table 2 are selected.

The five cases in Table 2 are designed with the following rationale: a reference case, with a fill ratio of 10%, achieves the best balance in dissipation between tangential and normal components in the context of the Emax mill (see Fig. 2(d)). Cases favoring tangential dissipation use a fill ratio of 6%, while those favoring normal dissipation use a fill ratio of 17%. It is worth highlighting that, until now, the influence of the fill ratio on the mechanochemical regeneration of $NaBH_4$ has not been investigated at all, let alone with a mechanistic rationale [15]. In broader mechanochemical research, this parameter is shifted for pragmatic or empirical reasons, making it unclear whether the reported results on mechanochemical yield arise from altered power input, modified collision modes, or both [38,39]. To account for the effects of these different fill ratios on the system's dynamics and mechanical behavior, two approaches are introduced: constant rotational speed and constant total power. Using both approaches, we can introduce a systematic exploration of the effects of the fill ratio in a mechanochemical reaction by enforcing power equivalence, providing a controlled platform for mechanistic interpretation.

State-of-the-art mechanochemical studies are typically carried out using only the constant rotational speed approach, where the mill speed stays fixed while the fill ratio is adjusted. Varying the fill ratio changes the total power dissipation because both the mass in the jar (number of milling balls) and the collision frequency shift. As stated above, the problem is that any change in reaction outcome now combines two effects: tangential vs. normal distribution and total power, making it impossible to determine which factor drives the yield. To resolve this confounding, the constant power strategy can be used.

In the constant power approach, the machine's rotational speed is carefully adjusted using Eqs. (3) and (4) to maintain constant total power dissipation. Since ultimately the goal is to set $P_{tot,ref} = P_{tot,i}$, the aforementioned equations can be manipulated to arrive at Eq. (6).

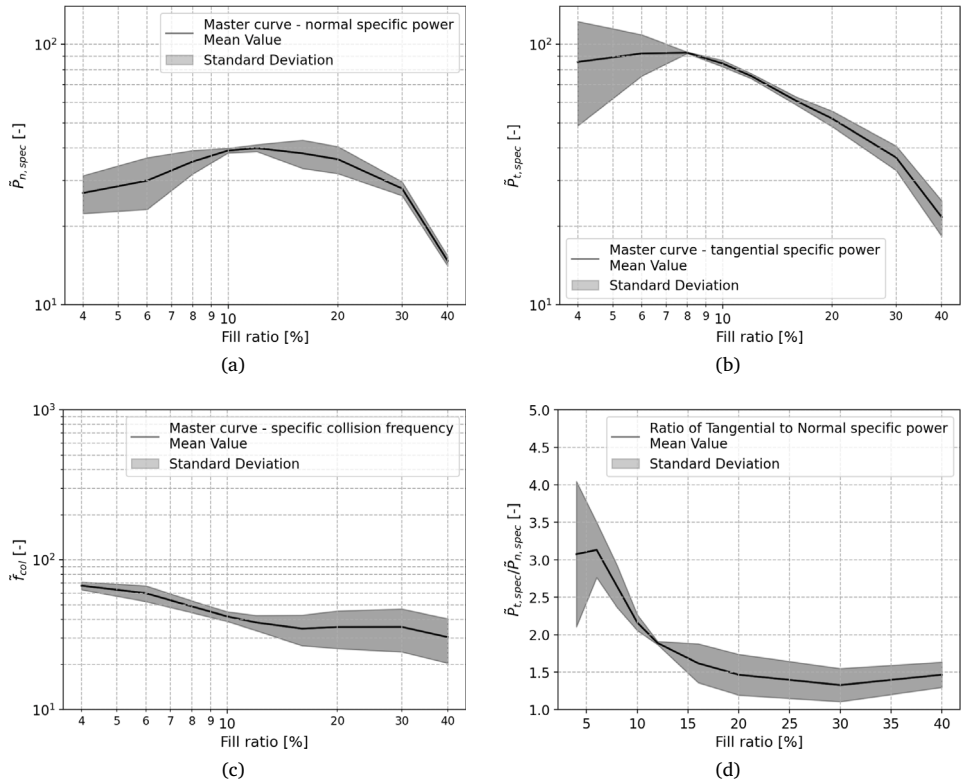

Fig. 2. (a) Master curve - mean specific normal power dissipation per collision $\tilde{P}_{spec,n}$ (b) Master curve - mean specific tangential power dissipation per collision $\tilde{P}_{spec,t}$ (c) Master curve - mean specific collision frequency $\tilde{f}_{col}$ (d) Ratio between mean specific tangential power dissipation per collision and mean specific normal power dissipation per collision $\tilde{P}_{spec,t}/\tilde{P}_{spec,n}$. Calibrated coefficients (system comprising $NaBO_2 \cdot 4\,H_2O$ and MgH_2). Figure reused from Garrido et al. [36], Powder Technology, 2025. This article is licensed under a Creative Commons Attribution 4.0 International License (CC BY 4.0).

Table 2
Comparison of milling scenarios at constant rotational speed versus constant total power. Two biased cases are shown for each operating mode: one that favors tangential dissipation and one that favors normal dissipation.

Parameter	Reference	Constant rot. speed		Constant total power	
	case	*Favor tang.*	*Favor norm.*	*Favor tang.*	*Favor norm.*
Fill ratio (%)	10	6	17	6	17
Rot. speed (Hz)	10.0	10.0	10.0	13.14	9.03
Spec. power, normal	39.7	23	43	23	43
Spec. power, tangential	90	75	60	75	60
Spec. collision frequency	40	70	25	70	25
Collision frequency (s^{-1}/n_{ball})	400	700	250	920	226
P_{tot} (W)	6.9	3.0	9.4	6.9	6.9
Normal energy (10^{-4} J)	2.21	0.73	3.82	1.26	3.12
Tangential energy (10^{-4} J)	5.00	2.38	5.34	4.11	4.35
Ratio tang./norm.	2.26	3.26	1.40	3.26	1.39
Mechanochemical yield (%)	71	84	43	94	40

This step assumes that the ball material and diameter, as well as the machine's amplitude, remain unchanged. Nonetheless, the influence of these parameters can be readily implemented back into the expression if they are varied.

$$\omega_i = \omega_{\text{ref}} \left(\frac{n_{\text{ball,ref}}\, \tilde{P}_{\text{spec,ref}}}{n_{\text{ball},i}\, \tilde{P}_{\text{spec},i}} \right)^{1/3} \tag{6}$$

In both strategies, the tangential to normal dissipation ratio remains constant because it is set solely by the fill ratio. What changes is how the total power is delivered to the reactants. By keeping that power constant, any shift in yield reflects how the power is supplied, rather than how much the system receives (see Table 2). Furthermore, all cases have the following previously optimized chemical operational parameters: BPR of 30, molar ratio of 66% above the stoichiometric value (see Eq. (2)), milling time of 12.5 h, and stainless steel balls (1.4034 G100 DIN 5401) with a diameter of 10 mm [15]. Each case was carried out three times to ensure reproducibility.

3. Results and discussion

This section presents the results obtained when the relative contribution of tangential and normal collision modes inside the jar is systematically varied. Two complementary approaches were applied to isolate mechanical effects. The first follows constant rotational speed, and the second follows constant total mechanical power. Alongside the absolute regeneration yield, each run is evaluated through its specific yield (W^{-1}), which relates fractional conversion yield directly to the mechanical power consumed, and through the converted mass per Watt (g W^{-1}), which relates net product output directly to the mechanical power consumed. Finally, we estimate mechanochemical

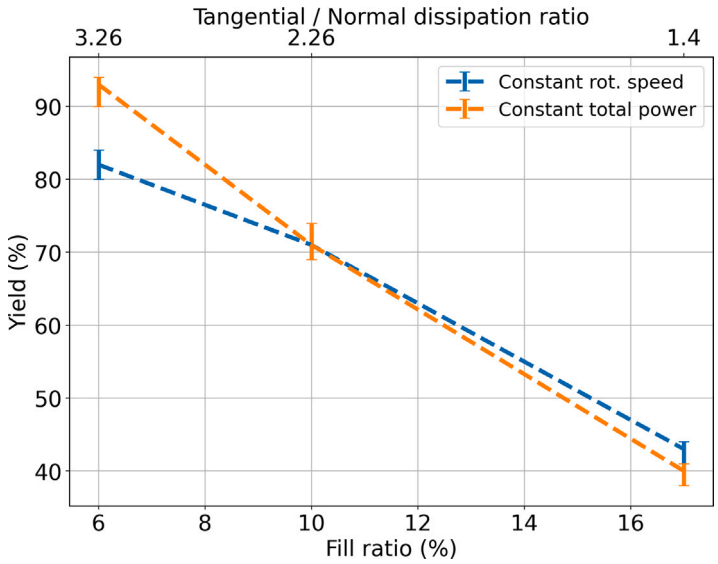

Fig. 3. Yield versus fill ratio for experiments run at constant rotational speed (blue) and at constant total mechanical power (orange). The secondary (top) axis converts each fill ratio to the corresponding tangential/normal dissipation ratio inside the jar. Error bars show the variability in yield.

Table 3
Mechanochemical regeneration of $NaBH_4$ from $NaBO_2 \cdot 4H_2O$ + MgH_2: prior art (Chen et al. 2017 [26]) and this work.

Metric	Chen et al. 2017 [26]	This work	Change
Regeneration yield (%)	88	94	+6%
Milling time (h)	20	12.5	−38%
Ball-to-powder ratio (BPR)	50	30	−40%
Rotational speed (Hz)	20	13.14	−34%

energy leverage metrics λ_{mc}, which measure the fraction of mechanical energy converted into recoverable chemical energy.

3.1. Tangential to normal dissipation ratio

The results in Fig. 3 depict how the conversion yield changes with fill ratio, which dictates the ratio between tangential and normal stressing events in the milling machine. In both approaches, the lowest fill (6%) leading to the highest tangential contribution gives the best performance. Under constant power operation, this achieves a regeneration yield of 94%, the highest value reported to date for the $NaBO_2 \cdot 4\,H_2O$ and MgH_2 system. Specifically, this is achieved while reducing the milling time by 38%, the ball-to-powder ratio by 40% (meaning more powder can be treated within the same batch), and the rotational speed by 34% (see Table 3) [26]. These gains demonstrate the potential for optimizing mechanochemical reactions with a deeper understanding of interactions among variables and the influence of mechanical conditions on the system.

When the system is held at constant speed, the tangential biased case still leads, but the yield is about ten percentage points lower than in the constant power approach. For normal-dominant cases, the opposite trend appears; constant speed offers a small advantage of less than five percentage points. A simple first-order model captures this behavior with high fidelity. Linear regression of yield against fill ratio gives $R^2 > 0.99$ for both approaches. The fitted slopes quantify the penalty for reducing tangential influence: yield falls by ≈0.038 per percentage of fill ratio at constant speed and by ≈0.049 per percentage of fill ratio at constant power, the latter being about 30% steeper. Thus, increasing fill ratio from 6% to 17% lowers the yield by roughly 0.4–0.5 (40–50 percentage points) regardless of the strategy.

For $NaBO_2 \cdot xH_2O + MgH_2 \longrightarrow NaBH_4$, solid-state studies support a stepwise interfacial hydride-substitution pathway: $[B(OH)_4]^-$ converts via a borohydride–hydroxy intermediate ($BH_3(OH)^-$/'$NaBH_3OH$') before full formation of BH_4^-, with ^{11}B MAS NMR directly detecting the intermediate under high-energy milling [26,40]. Accordingly, milling modes that maximize shear contact at reactive interfaces, continually renewing MgH_2/borate surfaces and abrading passivation layers (e.g., MgO, $Mg(OH)_2$), are more productive per Watt than brief head-on impacts (see Table 4 and Fig. 4). The advantage of a tangential-rich regime is consistent with known shear-activation channels in mechanochemistry [41]; it increases defect density and freshly created surface area, accelerates intimate mixing at reactive interfaces, and thereby can lower effective barriers for B–H bond-forming steps towards BH_4^-.

Across the different operating conditions tested, the highest specific yield performance is achieved when tangential dissipation dominates. Under the constant rotational speed regime, the mill reaches a specific yield of 0.28 (W^{-1}), which is 2.7 times higher than the balanced reference. Even when total mechanical power is held fixed at 6.9 W, simply reorienting collisions from normal to tangential raises the specific yield from 0.058 to 0.136 (W^{-1}), delivering a 134% jump in productivity without any additional energy input. By contrast, normal biased operation is doubly penalized as it demands more power (9.4 W versus 6.9 W) yet still depresses specific yield from 0.058 to 0.046 (W^{-1}).

It is also worth noting that, once tangential bias has driven the yield into the mid-80% range, further gains become increasingly expensive. Raising the yield from 84% (3 W) to 94% (6.9 W) requires more than doubling the mechanical power input, and the specific yield is reduced by 55%, illustrating clear diminishing returns as the process approaches full conversion. Expressing performance as converted mass per Watt (g W^{-1}) (see Table 4) gives a direct, quantitative metric to penalize these diminishing returns. Because the ball-to-powder ratio is constant, increasing the fill ratio processes more total reactant mass per batch, so even if a higher fill ratio yields a lower percentage conversion, the mass converted per Watt can still be greater. Framing conversion this way automatically penalizes those marginal, last percentage point gains that demand disproportionately more power; this can be visualized in Fig. 5.

While the constant rotational speed tangential run retains the highest conversion, its advantage shrinks to 64% compared to the reference case once the smaller batch mass is accounted for (see Table 4). Critically, in the constant mechanical power approach, the normal mode run overtakes its tangential counterpart on a mass per Watt basis (0.108

Table 4
Yield normalized by total mechanical power input for the five experimental conditions. The "specific yield" column (W^{-1}) measures the fractional conversion yield per Watt and is benchmarked against the balanced reference case. The "converted mass per Watt" measures the net mass conversion per mechanical power unit (g W^{-1}) and is also benchmarked against the balanced reference case.

Condition (orientation · fill · # balls)	P_{tot} (W)	Yield	Specific yield (W^{-1})	Gain vs. ref. (%)	$NaBO_2 \cdot 4H_2O$ mass (g)	Converted mass per Watt (g W^{-1})	Gain vs. ref. (%)
Reference – balanced · 10% · 24	6.9	0.71	0.103	–	1.10	0.113	–
Tangential favored – 6% · 14	3.0	0.84	0.280	+172	0.66	0.185	+64
Normal favored - 17% · 41	9.4	0.43	0.046	−56	1.87	0.086	−24
Tangential favored – 6% · 14	6.9	0.94	0.136	+32	0.66	0.090	−20
Normal favored - 17% · 41	6.9	0.40	0.058	−44	1.87	0.108	−4

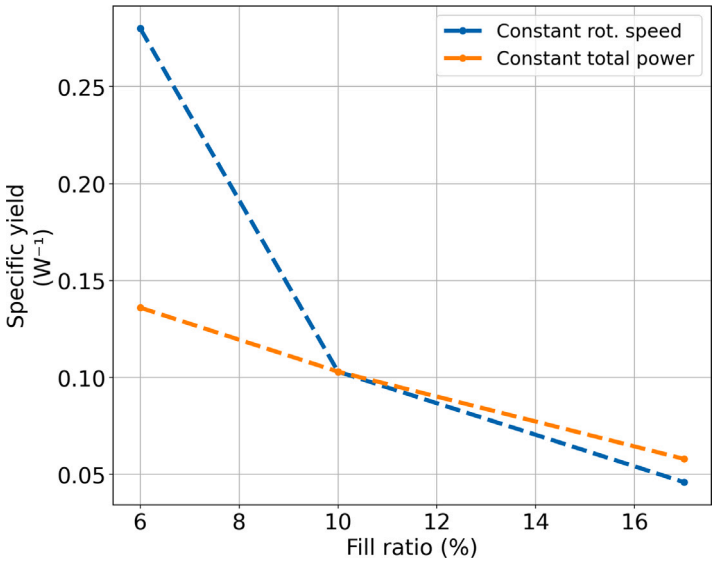

Fig. 4. Specific yield (W^{-1}) versus fill ratio for experiments run at constant rotational speed (blue) and at constant total mechanical power (orange).

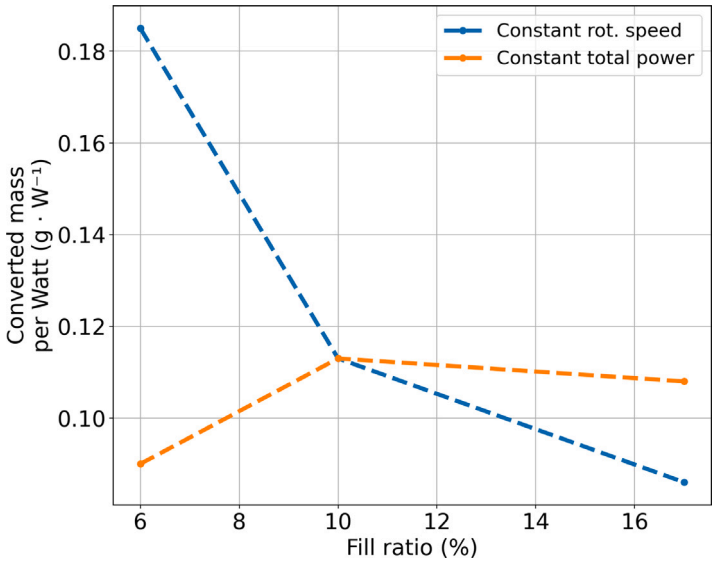

Fig. 5. Converted mass per W (g W^{-1}) versus fill ratio for experiments run at constant rotational speed (blue) and at constant total mechanical power (orange).

Table 5
Mechanochemical energy leverage λ_{mc} for each milling condition.

Operating conditions	$\lambda_{mc}(\Delta H)$%	$\lambda_{mc}(\Delta G)$%	$\lambda_{mc}(LHV)$%
Tangential favored – 6% · 3 W	3.65	4.49	8.66
Reference balanced – 10% · 6.9 W	2.24	2.75	5.30
Normal favored – 17% · 9.4 W	1.69	2.08	4.00
Tangential favored – 6% · 6.9 W	1.78	2.19	4.21
Normal favored – 17% · 6.9 W	2.14	2.64	5.08

vs. 0.090 g W^{-1}), and both perform worse than the balanced mode at 0.113 g W^{-1}. This result emphasizes a trade-off typically ignored in mechanochemical processes: while the net conversion efficiency reaches its peak (94%) under these tangential-rich conditions, the mechanical energetic cost to achieve the conversion renders the mass per Watt less attractive. The choice of operational conditions, therefore, depends on whether the goal is to maximize absolute percentage conversion or mass per Watt conversion.

3.2. Mechanochemical energy leverage

By quantifying the mechanical energy dissipated during the mechanochemical process, we can estimate the theoretical maximum of recaptured chemical energy in the regenerated $NaBH_4$, and the liberated H_2 (see Eq. (2)). For this, we define mechanochemical energy leverage (λ_{mc}) in Eq. (7):

$$\lambda_{mc} = \frac{E_{\text{chem}}}{E_{\text{mech}}} \tag{7}$$

where E_{mech} is the available mechanical energy defined as $P_{tot} \cdot t_{mill}$, with P_{tot} calculated via Eq. (5) and t_{mill} the milling time (in our case 12.5 h), and where E_{chem} is the chemical energy associated with $NaBH_4$ produced, evaluated on three baselines: the reaction enthalpy ΔH (−1226 kJ/mol), the Gibbs free energy ΔG (−1510 kJ/mol at 298 K), or the lower heating value LHV of H_2 available per cycle (2908 kJ/mol). Note that because λ_{mc} is referenced to the mechanical power dissipated inside the jar, it will overestimate the wall-plug efficiency. A formal techno-economic analysis is outside the scope of this study; nonetheless, the corresponding wall-plug specific energy intensity ($\bar{E}_{\text{plug}}$) and cost per kilogram of $NaBH_4$ (C_{NaBH_4}) can be estimated with Eqs. (8) and (9).

$$\bar{E}_{\text{plug}}\,[\text{kWh kg}^{-1}] = \frac{E_{mech}}{\eta_{\text{plug}}\, m_{NaBH_4}}, \tag{8}$$

$$C_{NaBH_4}\,[e\ \text{kg}^{-1}] = \bar{E}_{\text{plug}}\, p_{\text{elec}}, \tag{9}$$

where m_{NaBH_4} is the mass produced (kg), η_{plug} the electromechanical efficiency, and p_{elec} the electricity price (€/kWh).

The three comparison baselines form an energy quality hierarchy. The reaction enthalpy represents low-grade heat recoverable at room temperature; the Gibbs free energy is 1.23 × larger because it includes the maximum reversible work associated with the entropy gain, and the LHV is 2.37 × larger than $|\Delta H|$ because it accounts for the usable fuel energy stored in the liberated hydrogen and the regenerated $NaBH_4$. With E_{mech} fixed, λ_{mc} scales by the same factors (see Table 5). This shows how much of the invested work can be exploited as the process moves from heat recovery towards full fuel utilization.

As expected, the ranking of operating conditions coincides with the mass per Watt conversion ranking. The mechanochemical energy leverage values reveal that only 1.7–3.7% of the input mechanical work is recovered when evaluated on an enthalpy basis, 2.1–4.4% on a Gibbs free energy basis, and 4–8.7% when considering the fuel value of all available hydrogen (both directly liberated H_2 and that stored in $NaBH_4$). The best performance across all metrics is achieved under tangential milling at low power. While these LHV efficiencies account for the total hydrogen yield, they represent theoretical maxima assuming costless extraction of hydrogen from $NaBH_4$ via hydrolysis. In practice, the energy costs associated with hydrolysis will reduce these leverage values below the reported range, making the actual recoverable energy storage efficiency lower than these estimates indicate.

For context, mechanocatalytic water splitting over NiO achieves ≈ 4% enthalpy-based efficiency [42], whereas planetary ball mill reduction of water by metallic Ti consumes 1.72 kWh m^{-3} [43]. That equates to ≈ 52 g kW^{-1} h^{-1}, or 0.052 g W^{-1} on a one-hour basis, which is two-to-four times lower than the 0.090–0.185 g W^{-1} obtained here for $NaBH_4$ regeneration. While the processes are different, the scarcity of performance data for $NaBH_4$ regeneration makes any deeper comparison impossible.

4. Conclusions

In this work, we present a methodology to steer the contributions of tangential (shear) and normal (compressive) loading events during mechanochemical ball milling, specifically for the regeneration of $NaBH_4$. By combining DEM-derived mechanical descriptors with two complementary experimental approaches, one at constant rotational speed and one at constant total power, we separate changes in the energy dissipation distribution between tangential and normal modes from changes in overall collision dynamics. Because the dissipated energy in each mode scales with the corresponding contact forces, this distribution provides a practical and quantitative representation for the underlying stress landscape. Benchmarking each scenario through the specific yield (W^{-1}), the converted mass per Watt (g W^{-1}), and the mechanochemical energy leverage (λ_{mc}) offers relevant metrics for optimization and scale-up.

A low fill ratio of 6%, which maximizes tangential dissipation, is the clear optimum across both approaches if absolute percentage conversion is to be maximized. Under constant-power operation, it delivers a record 94% regeneration yield while reducing milling time by 38%, the ball-to-powder ratio by 40%, and the rotational speed by 34% compared to prior literature. The same tangential-rich state achieved at around half the power (3 W) attains 84% yield, giving a specific yield of 0.28 W^{-1}, five times the normal-dominant cases. Yield falls linearly with fill ratio ($R^2 > 0.99$), with gradients of 0.038 per percentage point at constant speed and 0.049 per point at constant power; thus, raising the fill from 6% to 17% costs 0.4–0.5 of fractional yield (40–50 percentage points) regardless of experimental approach. Together, these trends indicate that shear-dominated contact mechanics, rather than normal impacts, govern the rate-limiting interfacial chemistry. To mechanistically ground this, Density Functional Theory (DFT) derived energetics for the elementary steps could seed a microkinetic model that quantitatively links mechanical stress components (normal vs. tangential) to interfacial reaction rates, enabling prediction of optimal operating windows.

Our analysis further reveals that while tangential bias maximizes absolute conversion yield, mechanical energy cost and BPR diminish per-Watt mass conversion efficiency. Under constant mechanical power conditions, the balanced regime (10% fill) yields the highest converted mass per Watt (0.113 g W^{-1}) compared to both tangential (0.090 g W^{-1}) and normal (0.108 g W^{-1}) biased cases. This trade-off highlights that the optimal operating point depends on the prioritization of absolute conversion efficiency or normalized productivity.

The mechanochemical energy leverage of the process reveals theoretical maxima of 1.7–3.7% on an enthalpy basis, 2.1–4.4% on a Gibbs free energy basis, and 4–8.7% when considering the fuel value of all available hydrogen. These values indicate that the majority of input mechanical work is dissipated as heat and deformation rather than being converted to useful chemical energy. This inefficiency suggests opportunities for improving the process via thermal management, catalytic additives, or alternative reactor geometries that better harness mechanical work for chemical activation.

Taken together, these findings demonstrate the critical role of stress mode partitioning in mechanochemical reactions. Because the

three mechanical descriptors $\{\bar{E}_n, \bar{E}_t, f_{\mathrm{col}}/n_{\mathrm{ball}}\}$ are transferable between mills, any reactor that reproduces the tangential-rich scenarios identified here is expected to achieve comparable yields, provided other thermochemical factors (jar atmosphere, contamination, etc.) are controlled. By targeting desired mechanical conditions, practitioners can rationally design milling protocols to maximize yield, throughput, and energy efficiency.

CRediT authorship contribution statement

Santiago Garrido Nuñez: Writing – review & editing, Writing – original draft, Visualization, Validation, Software, Methodology, Investigation, Formal analysis, Data curation, Conceptualization. **Dingena L. Schott:** Writing – review & editing, Supervision, Conceptualization. **Johan T. Padding:** Writing – review & editing, Supervision, Funding acquisition, Formal analysis, Conceptualization.

Funding

This work was supported by the project SH2IPDRIVE: Sustainable Hydrogen Integrated Propulsion Drives, The Netherlands, funded by the RVO, The Netherlands under grant MOB21013.

Declaration of competing interest

The authors declare the following financial interests/personal relationships which may be considered as potential competing interests: Johan T. Padding reports financial support was provided by Dutch Research Council. If there are other authors, they declare that they have no known competing financial interests or personal relationships that could have appeared to influence the work reported in this paper.

Data availability

Data will be made available on request.

References

[1] E.S. van Rheenen, J.T. Padding, A.A. Kana, K. Visser, Comparative energy analysis of hydrogen carriers as energy source on ships, J. Mar. Eng. Technol. (2025) 1–15, http://dx.doi.org/10.1080/20464177.2024.2448057.

[2] E.Y. Marrero-Alfonso, A.M. Beaird, T.A. Davis, M.A. Matthews, Hydrogen generation from chemical hydrides, Ind. Eng. Chem. Res. 48 (8) (2009) 3703–3712, http://dx.doi.org/10.1021/ie8016225, arXiv:https://doi.org/10.1021/ie8016225.

[3] U. Demirci, O. Akdim, P. Miele, Ten-year efforts and a no-go recommendation for sodium borohydride for on-board automotive hydrogen storage, Int. J. Hydrog. Energy 34 (6) (2009) 2638–2645, http://dx.doi.org/10.1016/j.ijhydene.2009.01.038, URL https://www.sciencedirect.com/science/article/pii/S0360319909000603.

[4] Y. Zhu, L. Ouyang, H. Zhong, J. Liu, H. Wang, H. Shao, Z. Huang, M. Zhu, Closing the loop for hydrogen storage: Facile regeneration of NaBH4 from its hydrolytic product, Angew. Chem. Int. Ed. 59 (22) (2020) 8623–8629, http://dx.doi.org/10.1002/anie.201915988, arXiv:https://onlinelibrary.wiley.com/doi/pdf/10.1002/anie.201915988, URL https://onlinelibrary.wiley.com/doi/abs/10.1002/anie.201915988.

[5] H. Zhong, L.Z. Ouyang, J.S. Ye, J.W. Liu, H. Wang, X.D. Yao, M. Zhu, An one-step approach towards hydrogen production and storage through regeneration of NaBH4, Energy Storage Mater. 7 (2017) 222–228, http://dx.doi.org/10.1016/j.ensm.2017.03.001, URL https://www.sciencedirect.com/science/article/pii/S2405829717300302.

[6] H. Nunes, D. Silva, C. Rangel, A. Pinto, Rehydrogenation of sodium borates to close the $NaBH_4$-H_2 cycle: A review, Energies 14 (2021) 3567, http://dx.doi.org/10.3390/en14123567.

[7] H.N. Abdelhamid, A review on hydrogen generation from the hydrolysis of sodium borohydride, Int. J. Hydrog. Energy 46 (1) (2021) 726–765, http://dx.doi.org/10.1016/j.ijhydene.2020.09.186, URL https://www.sciencedirect.com/science/article/pii/S0360319920336260.

[8] H. Zhong, L. Ouyang, M. Zeng, J. Liu, H. Wang, H. Shao, M. Felderhoff, M. Zhu, Realizing facile regeneration of spent NaBH4 with Mg–Al alloy, J. Mater. Chem. A 7 (2019) 10723–10728, http://dx.doi.org/10.1039/C9TA00769E.

[9] M. Huang, H. Zhong, L. Ouyang, C. Peng, X. Zhu, W. Zhu, F. Fang, M. Zhu, Efficient regeneration of sodium borohydride via ball milling dihydrate sodium metaborate with magnesium and magnesium silicide, J. Alloys Compd. 729 (2017) 1079–1085, http://dx.doi.org/10.1016/j.jallcom.2017.09.262, URL https://www.sciencedirect.com/science/article/pii/S0925838817333121.

[10] S. Shen, L. Ouyang, From borate to borohydride: Achieving a high-yield synthesis of magnesium borohydride enabled by cation tuning, ACS Sustain. Chem. Eng. 13 (7) (2025) 2933–2942, http://dx.doi.org/10.1021/acssuschemeng.4c09817, arXiv:https://doi.org/10.1021/acssuschemeng.4c09817.

[11] K. Chen, H. Zhong, L. Ouyang, F. Liu, H. Wang, J. Liu, H. Shao, M. Zhu, Achieving a novel solvent-free regeneration of LiBH4 combining hydrogen storage and production in a closed material cycle, J. Magnes. Alloy. 11 (5) (2023) 1697–1708, http://dx.doi.org/10.1016/j.jma.2021.08.005, URL https://www.sciencedirect.com/science/article/pii/S2213956721002036.

[12] K. Chen, L. Ouyang, H. Zhong, J. Liu, H. Wang, H. Shao, Y. Zhang, M. Zhu, Converting H+ from coordinated water into H- enables super facile synthesis of LiBH4, Green Chem. 21 (2019) 4380–4387, http://dx.doi.org/10.1039/C9GC01897B.

[13] L. Ouyang, J. Jiang, K. Chen, M. Zhu, Z. Liu, Hydrogen production via hydrolysis and alcoholysis of light metal-based materials: A review, Nano-Micro Lett. 13 (1) (2021) 134, http://dx.doi.org/10.1007/s40820-021-00657-9.

[14] H. Zhong, K. Chen, C. Qin, C. Lang, J. Liu, H. Wang, J. Zhang, L. Ouyang, Enhancing NaBH4 regeneration using an Al-rich alloy, J. Alloys Compd. 976 (2024) 173160, http://dx.doi.org/10.1016/j.jallcom.2023.173160, URL https://www.sciencedirect.com/science/article/pii/S0925838823044638.

[15] S. Garrido Nuñez, D.L. Schott, J.T. Padding, Optimization of operational parameters in the mechanochemical regeneration of sodium borohydride (NaBH4), Int. J. Hydrog. Energy 97 (2025) 640–648, http://dx.doi.org/10.1016/j.ijhydene.2024.11.360, URL https://www.sciencedirect.com/science/article/pii/S0360319924050511.

[16] J. Batteas, K.G. Blank, E. Colacino, F. Emmerling, T. Friščić, J. Mack, J. Moore, M.E. Rivas, W. Tysoe, Moving mechanochemistry forward, RSC Mechanochem. 2 (2025) 10–19, http://dx.doi.org/10.1039/D4MR90021A.

[17] S.V. Sukhomlinov, G. Kickelbick, M.H. Müser, Mechanochemical ionization: Differentiating pressure-, shear-, and temperature-induced reactions in a model phosphate, Tribol. Lett. 70 (4) (2022) 102, http://dx.doi.org/10.1007/s11249-022-01644-w.

[18] H. Kobayashi, Y. Suzuki, T. Sagawa, K. Kuroki, J.-y. Hasegawa, A. Fukuoka, Impact of tensile and compressive forces on the hydrolysis of cellulose and chitin, Phys. Chem. Chem. Phys. 23 (2021) 15908–15916, http://dx.doi.org/10.1039/D1CP01650D.

[19] R. Rana, N. Hopper, F. Sidoroff, W.T. Tysoe, Critical stresses in mechanochemical reactions, Chem. Sci. 13 (2022) 12651–12658, http://dx.doi.org/10.1039/D2SC04000J.

[20] F.H. Bhuiyan, Y.-S. Li, S.H. Kim, A. Martini, Shear-activation of mechanochemical reactions through molecular deformation, Sci. Rep. 14 (1) (2024) 2992, http://dx.doi.org/10.1038/s41598-024-53254-2.

[21] C.-L. Hsueh, C.-H. Liu, B.-H. Chen, C.-Y. Chen, Y.-C. Kuo, K.-J. Hwang, J.-R. Ku, Regeneration of spent-NaBH 4 back to NaBH 4 by using high-energy ball milling, Int. J. Hydrog. Energy - Int. J. Hydrogen Energy 34 (2009) 1717–1725, http://dx.doi.org/10.1016/j.ijhydene.2008.12.036.

[22] L. Kong, C. Xinyu, H. Jin, J. Wu, H. Du, T. Xiong, Mechanochemical synthesis of sodium borohydride by recycling sodium metaborate, Energy Fuels - Energy Fuel 23 (2009) http://dx.doi.org/10.1021/ef900619y.

[23] C. Cakanyildirim, M. Gürü, Processing of NaBH4 from NaBO2 with MgH2 by ball milling and usage as hydrogen carrier, Renew. Energy 35 (2010) 1895–1899, http://dx.doi.org/10.1016/j.renene.2010.01.001.

[24] C. Lang, Y. Jia, J. Liu, H. Wang, L. Ouyang, M. Zhu, X. Yao, NaBH 4 regeneration from NaBO 2 by high-energy ball milling and its plausible mechanism, Int. J. Hydrog. Energy 42 (2017) http://dx.doi.org/10.1016/j.ijhydene.2017.04.014.

[25] L. Ouyang, W. Chen, J. Liu, M. Felderhoff, H. Wang, M. Zhu, Enhancing the regeneration process of consumed NaBH 4 for hydrogen storage, Adv. Energy Mater. 7 (2017) 1700299, http://dx.doi.org/10.1002/aenm.201700299.

[26] W. Chen, L. Ouyang, J. Liu, X. Yao, H. Wang, Z. Liu, M. Zhu, Hydrolysis and regeneration of sodium borohydride (NaBH 4) – A combination of hydrogen production and storage, J. Power Sources 359 (2017) 400–407, http://dx.doi.org/10.1016/j.jpowsour.2017.05.075.

[27] L. Fang, S. Korres, W.A. Lamberti, M.N. Webster, R.W. Carpick, What stress components drive mechanochemistry? A study of ZDDP tribofilm formation, Faraday Discuss. 241 (2023) 394, http://dx.doi.org/10.1039/D2FD00123C, URL https://pubs.rsc.org/en/content/articlelanding/2023/FD/D2FD00123C.

[28] J.L. Howard, Q. Cao, D.L. Browne, Mechanochemistry as an emerging tool for molecular synthesis: what can it offer? Chem. Sci. 9 (2018) 3080–3094, http://dx.doi.org/10.1039/C7SC05371A, URL https://pubs.rsc.org/en/content/articlehtml/2018/sc/c7sc05371a, Open Access.

[29] S. Rosenkranz, S. Breitung-Faes, A. Kwade, Experimental investigations and modeling of the ball motion in planetary ball mills, Powder Technol. 212 (2011) 224–230, http://dx.doi.org/10.1016/j.powtec.2011.05.021.

[30] C. Burmeister, M. Hofer, P. Molaiyan, P. Michalowski, A. Kwade, Characterization of stressing conditions in a high energy ball mill by discrete element simulations, Processes 10 (2022) 692, http://dx.doi.org/10.3390/pr10040692.

[31] C. Burmeister, R. Schmidt, K. Jacob, S. Breitung, A. Stolle, A. Kwade, Effect of stressing conditions on mechanochemical knoevenagel synthesis, Chem. Eng. J. 396 (2020) 124578, http://dx.doi.org/10.1016/j.cej.2020.124578.

[32] C.F. Burmeister, A. Stolle, R. Schmidt, K. Jacob, S. Breitung-Faes, A. Kwade, Experimental and computational investigation of knoevenagel condensation in planetary ball mills, Chem. Eng. Technol. 37 (5) (2014) 857–864, http://dx.doi.org/10.1002/ceat.201300738, arXiv:https://onlinelibrary.wiley.com/doi/pdf/10.1002/ceat.201300738, URL https://onlinelibrary.wiley.com/doi/abs/10.1002/ceat.201300738.

[33] A. Krusenbaum, S. Grätz, G.T. Tigineh, L. Borchardt, J.G. Kim, The mechanochemical synthesis of polymers, Chem. Soc. Rev. 51 (7) (2022) 2873–2905, http://dx.doi.org/10.1039/d1cs01093j.

[34] S. Pagola, Outstanding advantages, current drawbacks, and significant recent developments in mechanochemistry: A perspective view, Crystals 13 (1) (2023) http://dx.doi.org/10.3390/cryst13010124, URL https://www.mdpi.com/2073-4352/13/1/124.

[35] R.T. O'Neill, R. Boulatov, The many flavours of mechanochemistry and its plausible conceptual underpinnings, Nat. Rev. Chem. 5 (3) (2021) 148–167, http://dx.doi.org/10.1038/s41570-020-00249-y.

[36] S. Garrido Nuñez, D.L. Schott, J.T. Padding, Predictive models for energy dissipation in mechanochemical ball milling, Powder Technol. 457 (2025) 120919, http://dx.doi.org/10.1016/j.powtec.2025.120919, URL https://www.sciencedirect.com/science/article/pii/S0032591025003146.

[37] S. Garrido Nuñez, D.L. Schott, J.T. Padding, Accelerating granular dynamics simulations: A graph neural network surrogate for complex high-energy ball milling, Powder Technol. 468 (2026) 121653, http://dx.doi.org/10.1016/j.powtec.2025.121653, URL https://www.sciencedirect.com/science/article/pii/S0032591025010484.

[38] O. Jafter, S. Lee, J. Park, C. Cabanetos, D. Lungerich, Navigating ball mill specifications for theory-to-practice reproducibility in mechanochemistry, Angew. Chem. Int. Ed. 63 (2024) e202409731, http://dx.doi.org/10.1002/anie.202409731.

[39] W. Pickhardt, S. Grätz, L. Borchardt, Direct mechanocatalysis: Using milling balls as catalysts, Chem. – A Eur. J. 26 (57) (2020) 12903–12911, http://dx.doi.org/10.1002/chem.202001177, arXiv:https://chemistry-europe.onlinelibrary.wiley.com/doi/pdf/10.1002/chem.202001177, URL https://chemistry-europe.onlinelibrary.wiley.com/doi/abs/10.1002/chem.202001177.

[40] L. Ouyang, H. Zhong, H.-W. Li, M. Zhu, A recycling hydrogen supply system of NaBH4 based on a facile regeneration process: A review, Inorg. 6 (1) (2018) URL https://www.mdpi.com/2304-6740/6/1/10.

[41] J. Lyu, A. Lider, V. Kudiiarov, Using ball milling for modification of the hydrogenation/dehydrogenation process in magnesium-based hydrogen storage materials: An overview, Metals 9 (7) (2019) http://dx.doi.org/10.3390/met9070768, URL https://www.mdpi.com/2075-4701/9/7/768.

[42] K. Domen, J.N. Kondo, M. Hara, T. Takata, Photo- and mechano-catalytic overall water splitting reactions to form hydrogen and oxygen on heterogeneous catalysts, Bull. Chem. Soc. Japan 73 (6) (2001) 1307–1331, http://dx.doi.org/10.1246/bcsj.73.1307, arXiv:https://academic.oup.com/bcsj/article-pdf/73/6/1307/56193956/bcsj.73.1307.pdf.

[43] T. Yamamoto, S. Ashida, N. Inubuse, S. Shimizu, Y. Miura, T. Mizutani, K.-i. Saitow, Room-temperature thermochemical water splitting: efficient mechanocatalytic hydrogen production, J. Mater. Chem. A 12 (2024) 30906–30918, http://dx.doi.org/10.1039/D4TA04650A.